physica status solidi rrl
www.pss-rapid.com

$Fe_{5-x}Ge_2Te_2$—a New Exfoliable Itinerant Ferromagnet with High Curie Temperature and Large Perpendicular Magnetic Anisotropy

*Palani R. Jothi, Jan P. Scheifers, Yuemei Zhang, Mohammed Alghamdi, Dejan Stekovic, Mikhail E. Itkis, Jing Shi, and Boniface P. T. Fokwa**

Layered van der Waals (vdW) crystals with intrinsic magnetic properties such as high Curie temperature (T_C) and large perpendicular magnetic anisotropy (PMA) are key to the development and application of spintronic devices. The ferromagnetic vdW metal $Fe_{3-x}GeTe_2$ (FGT) has gained prominence recently due to its high T_C (220 K) and strong PMA. Herein, a new metallic vdW ferromagnet, $Fe_{5-x}Ge_2Te_2$ or FG2T, is introduced, which is successfully synthesized and fully characterized. FG2T is a metal that orders ferromagnetically with a very sharp transition at 250 K (bulk and single-crystal thin flakes) and shows large PMA, as found by both experimental and computational studies. Novel heterostructure devices with near-room-temperature capabilities using FG2T as a spin injector are enabled by this work.

Layered van der Waals (vdW) materials have attracted a great deal of interest since the discovery of graphene through exfoliation of graphite.[1,2] The prospect of realizing nanoscale spintronic devices constructed from atomically thin 2D ferromagnetic (FM) materials through combination of large spin polarization and high Curie temperature (T_C) has propelled these materials to a high level of interest in the scientific community. The first intrinsically 2D FM materials were realized from exfoliation of the FM CrI_3 (insulator with bulk $T_C = 61$ K),[3] FM $Cr_2Ge_2Te_6$ (insulator with bulk $T_C = 60$ K),[4] and recently FM VI_3 (semiconductor with bulk $T_C = 50$ K).[5] However, T_C of these materials remains somewhat low for spintronic applications, thus creating new challenges for both experimentalists and theoreticians to search for new 2D intrinsic ferromagnets with much higher T_C. In contrast, itinerant FM vdW $Fe_{3-x}GeTe_2$ (FGT), discovered in 2006 by Deiseroth et al.,[6] has a high T_C ranging from 150 to 220 K (depending on Fe vacancy x)[6–10] and thus has recently attracted the attention of the scientific community. Although bulk FGT is already very interesting as an itinerant ferromagnet showing Kondo lattice behavior and large anomalous Hall current, among other properties,[6–9] it is the high T_C and the large perpendicular magnetic anisotropy (PMA) in thin films that have propelled this phase to prominence.[10] Even more impressive is the recent discovery of 2D itinerant ferromagnetism in the FGT monolayer with the highest reported T_C (130 K),[11] thus enabling the engineering of advanced spintronic vdW heterostructures. Some heterostructures have recently been realized by combining FGT with other vdW materials (h-BN, graphite) or metal thin films (Pt) to investigate various properties such as tunneling spin valves, antisymmetric magnetoresistance, and spin–orbit torques (SOT).[12] Although FGT has comparably high T_C, it is still below room temperature; however, it was recently demonstrated that an ionic gate (using Li^+ intercalation) or microstructures patterning (by a focused ion beam) can raise T_C of FGT thin flakes up to room temperature, thus creating further opportunities for room temperature spintronic devices based on atomically thin vdW crystals.[13] Nevertheless, it remains a challenge to find vdW crystals with high enough T_C that will enable the exfoliation of a monolayer with intrinsic above room temperature T_C, a prerequisite for any application. Johrendt and coworkers[14a] and McGuire and coworkers[14b] have recently found that another known vdW crystal in the Fe–Ge–Te system, $Fe_{5-x}GeTe_2$,[15] has an even higher T_C than FGT, with values of 290 and 310 K reported for the bulk crystals that show a high level of stacking fault disorder if compared with FGT crystals. $Fe_{5-x}GeTe_2$ structurally differs from FGT because it has an extra honeycomb iron layer that contributes to the additional iron in the chemical formula.

Dr. P. R. Jothi, J. P. Scheifers, Prof. Y. Zhang, Dr. D. Stekovic, Prof. M. E. Itkis, Prof. B. P. T. Fokwa
Department of Chemistry
University of California
Riverside, CA 92521, USA
E-mail: bfokwa@ucr.edu

Prof. Y. Zhang
Department of Chemistry
Warren Wilson College
Asheville, NC 28815, USA

M. Alghamdi, Prof. J. Shi
Department of Physics and Astronomy
University of California
Riverside, CA 92521, USA

Prof. M. E. Itkis
Department of Chemical and Environmental Engineering
University of California
Riverside, CA 92521, USA

The ORCID identification number(s) for the author(s) of this article can be found under https://doi.org/10.1002/pssr.201900666.

DOI: 10.1002/pssr.201900666

We report on a new vdW crystal in the Fe–Ge–Te system, $Fe_{5-x}Ge_2Te_2$ (FG2T), that has a higher T_C than FGT with a sharp FM transition at 250 K. Hall measurements on thin flake single crystals demonstrate large PMA, and resistivity measurements show metallic behavior. Density functional theory (DFT) calculations have confirmed the itinerant FM ground state as well as strong PMA for thin flakes.

Synthesis and crystal structure of $Fe_{4.84(1)}Ge_2Te_2$ (FG2T): FG2T was synthesized following a solid state reaction route from its elemental constituents. Two samples were submitted to different heat treatments: The first sample was annealed at 800 °C followed by slow cooling, which yielded a polycrystalline powder containing small crystals, while the second sample was quenched after annealing at 760 °C, leading to larger crystals. In both synthesis conditions, the obtained products contained FG2T as majority phase as exemplified by the Rietveld refinement conducted on the powder X-ray diffraction (PXRD) data (see Figure S1 and Table S1, Supporting Information, and the synthesis section in the Supporting Information). The crystal structure of FG2T was determined by single-crystal X-ray diffraction (SCXRD) from which the trigonal centrosymmetric space group $P\bar{3}m1$ (no. 164) was identified. The lattice parameters [$a = b = 4.0121(3)$ Å and $c = 10.7777(8)$ Å] obtained from the SCXRD analysis were in very good agreement with those from the two PXRD datasets (see Table S2, Supporting Information), indicating a uniform sample as confirmed by the refined chemical formulas in all cases. The refined structure has five main Wyckoff positions in its asymmetric unit [Te (site 2d), Ge (site 2d), Fe_1 (site 2d), Fe_2 (site 2c), and Fe_3 (site 1a)], leading to the initial chemical formula $Fe_5Ge_2Te_2$. However, a significant electron density was found at site 1b, and a free refinement of this site's occupancy with Fe (like in the case of Ni in $Ni_{3-x}GeTe_2$[5]) led to a partially occupied site (Fe_4) with an occupancy of 16.4(9) %. Also, in all related phases found until now, the 2d site (Fe_1) is always reported as partially occupied; thus we have refined this site, leading to an occupancy of only 83.8(7)%. Furthermore, we have observed enlarged (in the *ab* plane) anisotropic displacement parameters (ADPs) for Ge. In addition, small peaks in the electron density map were observed at ≈0.6 Å from Ge [also found in our electron localization function (ELF) analysis; cf. Figure S2, Supporting Information]. Introducing a split site for Ge (73% at 2d and 8.9% at 6i) resulted in improved *R*-values, decreased ADPs, and disappearance of the peaks in the electron density. The final refinement (see Table S3–S5, Supporting Information) led to excellent reliability values and a final composition of $Fe_{4.84(1)}Ge_2Te_2$, which is in perfect agreement with the refined compositions obtained from the Rietveld refinements of the two bulk samples (Table S2, Supporting Information). The presence of the three elements was further confirmed by semiquantitative energy-dispersive X-ray spectroscopy (EDS) done on several crystals (Figure S3, Supporting Information). In contrast to $Fe_{5-x}GeTe_2$,[14] we did not observe severe stacking disorder along [001] in any of the analyzed single crystals of FG2T (Figure S4, Supporting Information). The final crystal structure of FG2T is shown in **Figure 1**. The Wyckoff sequence *164,id²cba* indicates a new structure type. The new structure is built from slabs stacked along [001] and separated by a vdW gap of 2.886(2) Å, a value slightly smaller than those of FGT (2.95 Å)[6] and $Fe_{5-x}GeTe_2$ (3.06 Å).[14] Each FG2T slab consists of seven layers in the sequence ABCB′C′BA′: Three layers of Fe (Fe_2 in each of the two B and Fe_3 in B′) are stacked on top of each other, leading to face-sharing trigonal prisms of Fe_2 and Fe_3 atoms. These prisms are alternatingly filled by Fe_1 and Ge, resulting in the mixed Ge/Fe layers C and C′. The slab is terminated by a layer of Te on each side, namely, A and A′ layers. Due to the double layer of Fe prisms and the alternate arrangement of Ge and Fe_1 atoms within the double layer, the layers A and A′ of the same slab are offset to each other. This has two important consequences: 1) only a single slab is required per unit cell to achieve translational symmetry along [001] and

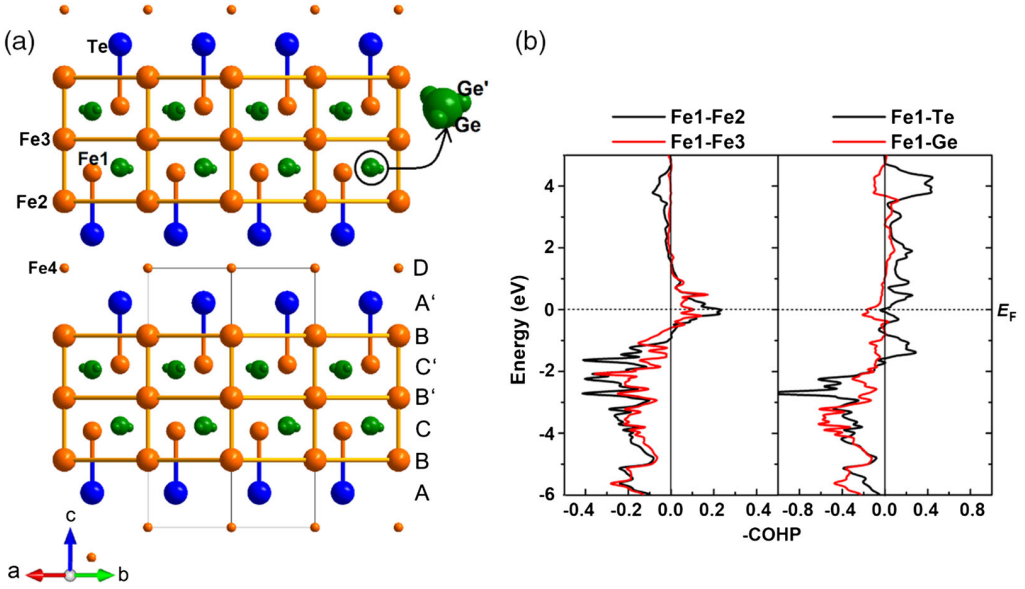

Figure 1. a) Projection along [110] of the crystal structure of $Fe_{5-x}Ge_2Te_2$. b) LDA-COHP curves for Fe-based interactions in $Fe_{5-x}Ge_2Te_2$. The relative sizes of the spheres represent the site occupation factor: 100% for Te, Fe_2, and Fe_3; 83.8% for Fe_1; 16.4% for Fe_4; 73% for Ge; and 8.9% for Ge′.

2) the Te atoms of two neighboring slabs form empty octahedra and tetrahedra at the vdW gap. In the center of the octahedra, we found significant electron density reflecting a partially occupied (16% Fe) atomic position at (0,0,0). We denote this layer D.

Examining the structure of FG2T ($Fe_{5-x}Ge_2Te_2$) more closely reveals that the layers C and C′ are not perfectly flat; that is, Fe_1 and Ge do not have the same *z*-coordinate. In fact, the Fe_1–Ge distance is rather short (2.325 Å on average), which is the reason for the vacancies on the Fe_1 site, the puckering of the layer, and the split site for Ge (in the *ab* plane). This contrasts with $Fe_{5-x}GeTe_2$,[14] where Ge is displaced along *c* instead of in the *ab* plane. The displacement of the Fe_1 atom toward the vdW gap increases the Fe_1–Ge distance and shortens the Fe_1–Te distance, which is even shorter than the shortest Fe_2–Te distance of 2.563(3) Å. The short Fe_1–Te distance reflects a strong bond, which explains why Te prefers to cap the Fe-filled trigonal prisms over the Ge-filled ones.

The FG2T structure is closely related to other layered tellurides and especially to FGT. The main difference between FGT and FG2T is the number of Ge/Fe layers building a slab: whereas FGT contains a thin slab of five layers centered around a single Ge/Fe layer C in a layer sequence ABCBA, FG2T exhibits a thicker seven-layer slab containing two Ge/Fe layers in a stacking sequence ABCB′C′BA′. Removing one Fe layer (B′) and one $Fe_{1-x}Ge$ layer (C′), i.e., one $Fe_{2-x}Ge$ block, from $Fe_{5-x}Ge_2Te_2$ would lead to the FGT composition.

Density functional theory results for FG2T: SCXRD of FG2T found partially occupied sites for Fe_1 (84%) and Fe_4 (16%) as well as a split site for Ge, all of which are not easy to simulate computationally. Therefore, a simplified model for $Fe_5Ge_2Te_2$, containing fully occupied Fe_1, no Fe_4, and no Ge split site (see Table S5, Supporting Information), was used for our DFT total energy calculations (see SI for details).[16,17] Density of states (DOS) from local density approximation (LDA) calculations (**Figure 2**, left) show a large density at the Fermi level (E_F), indicating electronic instability. By applying spin polarization [local spin density approximation (LSDA) calculations], the split of majority and minority spins opens a pseudogap at E_F (Figure 2, left), diminishes the electronic instability, and induces magnetic ordering. Moreover, there is no bandgap at E_F for both LDA and LSDA calculations, indicating a metallic behavior for $Fe_5Ge_2Te_2$, as confirmed by the transport measurements (Figure 2, bottom right). To explore the partial occupancy of Fe_1 site, chemical bonding analysis, using the crystal orbital Hamilton population (COHP)[18] curves (Figure 1, right), was applied for Fe_1–Fe_2, Fe_1–Fe_3, Fe_1–Te, and Fe_1–Ge interactions. Except for the Fe_1–Ge bond, all others have partially filled antibonding states. Fe_1 partial occupancy can decrease the number of these bonds because it reduces the valence electron count, which moves E_F to the left and reduces the filling of the antibonding region, thereby stabilizing the electronic structure. Consequently, partial occupancy of Fe_1 would be expected. In addition, E_F sits on a peak in the LDA-DOS and in the antibonding region of Fe_1–Fe_2 and Fe_1–Fe_3 COHP curves. Therefore, FM couplings are expected for Fe_1–Fe_2 and Fe_1–Fe_3 interactions according to the COHP interpretation of magnetic interactions,[19] suggesting FM ordering for this compound. Furthermore, we have calculated the total energy of two magnetic models, one with FM couplings within the slab and between slabs, another containing antiferromagnetically coupled FM slabs. Our results show that the first model is more stable than the second by 13.6 meV/f.u. Therefore, the interslab magnetic coupling in $Fe_5Ge_2Te_2$ is weak FM unlike in Fe_3GeTe_2 where antiferromagnetic coupling is more stable (our own calculations and others[9c]), indicating FM ordering in this new compound. Indeed, magnetic measurements have confirmed this finding (see below and Figure 2 and **3**).

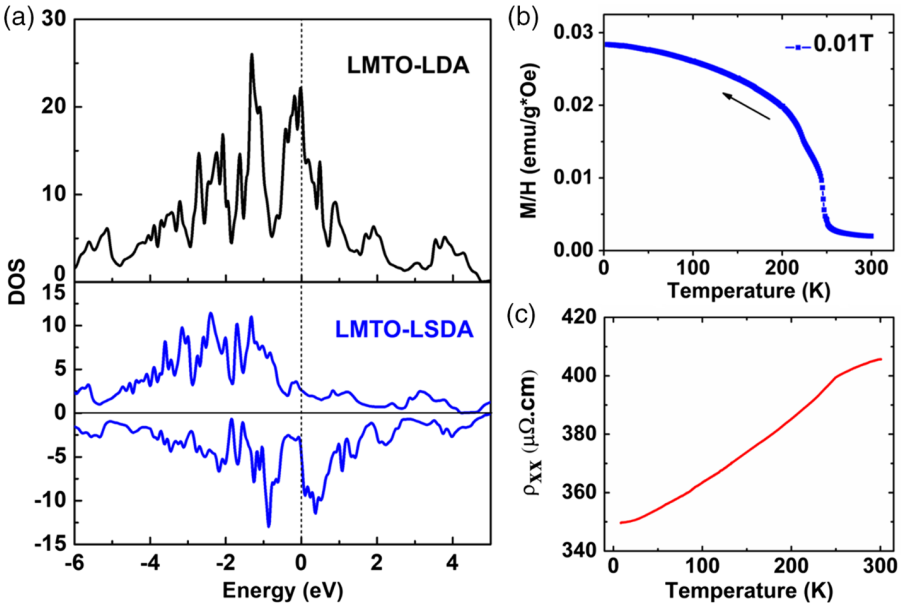

Figure 2. a) LDA and LSDA (from linear muffin-tin orbital code) DOS for $Fe_5Ge_2Te_2$. b) Temperature dependence of the magnetic susceptibility of a bulk $Fe_{5-x}Ge_2Te_2$ sample (containing a $Fe_{3-x}GeTe_2$ impurity, small inflection at ≈220 K). c) Temperature dependence of the longitudinal resistivity ρ_{xx} of a 125 nm-thick $Fe_{5-x}Ge_2Te_2$ single-crystal device.

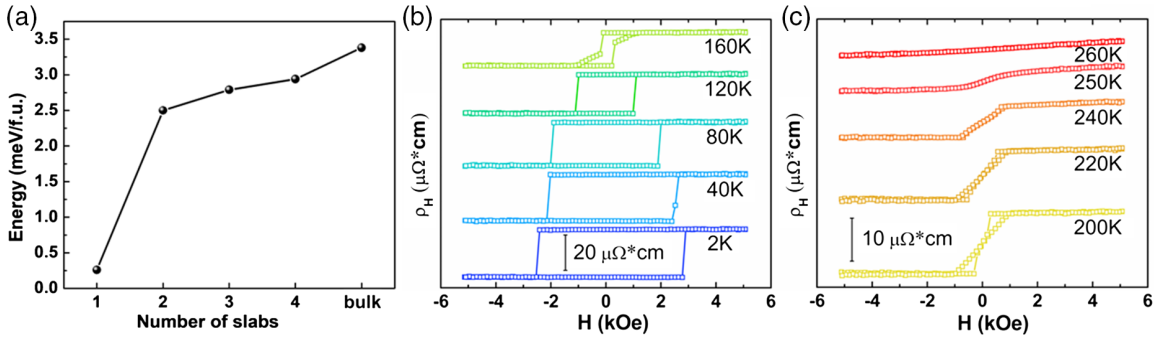

Figure 3. a) DFT-calculated MAE (absolute values) of $Fe_5Ge_2Te_2$ plotted as function of number of slabs. b,c) Hall resistivity as a function of applied field for a 114 nm thick single-crystal flake of $Fe_{5-x}Ge_2Te_2$ at temperatures from 2 to 260 K.

Lastly, the magnetic anisotropy of bulk and thin-film FG2T was studied using spin–orbit coupling (SOC) calculations. The magnetic anisotropy energy (MAE = $E_{SOC}(\|c) - E_{SOC}(\perp c)$) obtained for the bulk is −3.38 meV/f.u. (−3.6 MJ m^{-3}), indicating very strong easy axis anisotropy. MAE as a function of slab thickness was also examined for thin films. The results are shown in Figure 3 (left). The single layer has more than ten times weaker anisotropy compared with bulk $Fe_5Ge_2Te_2$. From a single layer to a two-layer film, the anisotropy increases dramatically and then slightly increases as the number of layers increases. Therefore, it is predicted that any $Fe_5Ge_2Te_2$ thin film with more than one slab would have large easy axis magnetic anisotropy. Indeed, the magnetotransport properties below on a 114 nm-thick sample confirm this prediction.

Magnetic, magnetotransport, and electrotransport properties of FG2T: The magnetic property measurements of the new FG2T phase were conducted on a polycrystalline sample. Figure 2 (top right) shows the temperature dependence magnetic susceptibility measurement in the temperature range 2–300 K and at an applied magnetic field of 0.01 T. The abrupt increase of susceptibility at ≈250 K (T_C) indicates a sharp ordering transition, as observed for strong ferromagnets, and hints at homogeneous composition throughout the sample (see aforementioned XRD analysis). Also, the earlier reported FGT impurity in this sample is found in this measurement, as an inflection is seen at ≈220 K (T_C of FGT). Consequently, the higher T_C value is due to the new FG2T phase, as further confirmed by transport measurements on single-crystal flakes below. The *M*–*H* curve (Figure S5, Supporting Information) recorded at 4 K shows a hysteresis with soft ferromagnet behavior for the FG2T polycrystalline sample, like FGT, and both materials become hard ferromagnets in thin flake single crystals (see the following).

The resistivity of a 125 nm FG2T single-crystal flake, shown in Figure 2 (bottom right), shows a slight decrease from 405 μΩ cm at 300 K to 400 μΩ cm at 252 K, and then a more rapid decrease to 350 μΩ cm at 2 K. The steep drop at 252 K coincides with the FM phase transition. The FG2T resistivity corresponds to metallic behavior, as predicted earlier by DFT. Similar resistivity values at 300 K have been reported for FGT (648[11] and 440 μΩ cm[9b]) and $Fe_{5-x}GeTe_2$ (300 μΩ cm[14b]). FG2T is therefore a FM metal, as predicted by DFT.

The recorded hysteresis loops of the anomalous Hall resistivity ρ_H for a single-crystal FG2T device with thickness 114 nm are shown in Figure 3 (middle and right) for different temperatures ranging from 2 to 260 K (device image is shown in the inset, Figure S6, Supporting Information). The ρ_H loops are squared from 2 up to 160 K with an increasing coercive field H_c as the temperature is decreased. H_c reaches ≈2.6 kOe at 2 K, indicating strong PMA, as predicted by DFT. Above 160 K, the ρ_H loops start to collapse and they disappear at ≈252 K (T_C). Simultaneously, the magnitude of ρ_H loops, i.e., the height between the two saturated values, decreases as the temperature is raised, and vanishes at the Curie temperature (252 K) as shown in Figure S6, Supporting Information. Another evaluation of T_c was performed using the Arrott plot, on the 114 nm device, which gave $T_C = 253.8$ K (Figure S7, Supporting Information). The overall temperature dependence of ρ_H of $Fe_{5-x}Ge_2Te_2$ resembles its mean-field magnetization (see Figure S6, Supporting Information), but it is slightly steeper.

In summary, we have discovered a new vdW material, $Fe_{5-x}Ge_2Te_2$ (FG2T), which was studied experimentally and theoretically. FG2T has a 30 K higher T_C than FGT and shows large PMA. Monolayer FG2T would be an interesting experimental target as it is expected to have a higher T_C value than FGT (130 K). Furthermore, we expect FG2T to enable fundamental physics through heterostructure and near-room-temperature spintronic device fabrications. During the review of this work, we became aware of the phase $Fe_{2.3}GeTe$ (CCSD 1953048), which has the same space group as FG2T and was reported as a conference proceeding abstract.[20]

Supporting Information

Supporting Information is available from the Wiley Online Library or from the author.

Acknowledgements

This work was supported by the startup fund to BPTF at UC Riverside and the National Science Foundation Career award to BPTF (no. DMR-1654780). The authors further acknowledge support by DOE BES Award No. DE-FG02-07ER46351 for device nanofabrication and transport measurements. The authors acknowledge UC Riverside's High-Performance Computing Center (HPCC) and the San Diego Supercomputing Center (XSEDE) for theoretical calculations.

Conflict of Interest

The authors declare no conflict of interest.

Keywords

density functional theory calculations, exfoliation, ferromagnetism, perpendicular magnetic anisotropy, van der Waals materials

Received: November 25, 2019
Published online:

[1] H. Li, S. Ruan, Y.-J. Zeng, *Adv. Mater.* **2019**, *31*, 1900065.
[2] M. Gibertini, M. Koperski, A. F. Morpurgo, K. S. Novoselov, *Nat. Nanotechnol.* **2019**, *14*, 408.
[3] B. Huang, G. Clark, E. N. Moratalla, D. R. Klein, R. Cheng, K. L. Seyler, D. Zhong, E. Schmidgall, M. A. McGuire, D. H. Cobden, W. Yao, D. Xiao, P. J. Herrero, X. Xu, *Nature* **2017**, *546*, 270.
[4] a) C. Gong, L. Li, Z. Li, H. Ji, A. Stern, Y. Xia, T. Cao, W. Bao, C. Wang, Y. Wang, Z. Q. Qiu, R. J. Cava, S. G. Louie, J. Xia, X. Zhang, *Nature* **2017**, *546*, 265; b) M. Lohmann, T. Su, B. Niu, Y. Hou, M. Alghamdi, M. Aldosary, W. Xing, J. Zhong, S. Jia, W. Han, R. Wu, Y.-T. Cui, J. Shi, *Nano Lett.* **2019**, *194*, 2397.
[5] a) T. Kong, K. Stolze, E. I. Timmons, J. Tao, D. Ni, S. Guo, Z. Yang, R. Prozorov, R. J. Cava, *Adv. Mater.* **2019**, *31*, 1808074; b) S. Tian, J.-F. Zhang, C. Li, T. Ying, S. Li, X. Zhang, K. Liu, H. Lei, *J. Am. Chem. Soc.* **2019**, *141*, 5326.
[6] H.-J. Deiseroth, K. Aleksandrov, C. Reiner, L. Kienle, R. K. Kremer, *Eur. J. Inorg. Chem.* **2006**, 1561.
[7] V. Y. Verchenko, A. A. Tsirlin, A. V. Sobolev, I. A. Presniakov, A. V. Shevelkov, *Inorg. Chem.* **2015**, *54*, 8598.
[8] a) A. F. May, S. Calder, C. Cantoni, H. Cao, M. A. McGuire, *Phys. Rev. B* **2016**, *93*, 014411; b) H. L. Zhuang, P. R. C. Kent, R. G. Hennig, *Phys. Rev. B* **2016**, *93*, 134407; c) N. León-Brito, E. D. Bauer, F. Ronning, J. D. Thompson, R. Movshovich, *J. Appl. Phys.* **2016**, *120*, 083903.
[9] a) B. Liu, Y. Zou, S. Zhou, L. Zhang, Z. Wang, H. Li, Z. Qu, Y. Zhang, *Sci. Rep.* **2017**, *7*, 6184; b) Y. Wang, C. Xian, J. Wang, B. Liu, L. Ling, L. Zhang, L. Cao, Z. Qu, Y. Xiong, *Phys. Rev. B* **2017**, *96*, 134428; c) J. Yi, H. Zhuang, Q. Zou, Z. Wu, G. Cao, S. Tang, S. A. Calder, P. R. C. Kent, D. Mandrus, Z. Gai, *2D Mater.* **2017**, *4*, 011005.
[10] a) C. Tan, J. Lee, S.-G. Jung, T. Park, S. Albarakati, J. Partridge, M. R. Field, D. G. McCulloch, L. Wang, C. Lee, *Nat. Commun.* **2018**, *9*, 1554; b) L. Luo, Z. Zhang, X. Lai, *Sci. Adv.* **2018**, *4*, eaao6791; c) K. Kim, J. Seo, E. Lee, K.-T. Ko, B. S. Kim, B. G. Jang, J. M. Ok, J. Lee, Y. J. Jo, W. Kang, J. H. Shim, C. Kim, H. W. Yeom, B. Min, B.-J. Yang, J. S. Kim, *Nat. Mater.* **2018**, *17*, 794; d) L. Luo, Z. Zhang, X. Lai, *Sci. Adv.* **2018**, *4*, eaao6791; e) K. Kim, J. Seo, E. Lee, K.-T. Ko, B. S. Kim, B. G. Jang, J. M. Ok, J. Lee, Y. J. Jo, W. Kang, J. H. Shim, C. Kim, H. W. Yeom, B. Min, B.-J. Yang, J. S. Kim, *Nat. Mater.* **2018**, *17*, 794; f) Y. Liu, E. Stavitski, K. Attenkofer, C. Petrovic, *Phys. Rev. B* **2018**, *97*, 165415.
[11] Z. Fei, B. Huang, P. Malinowski, W. Wang, T. Song, J. Sanchez, W. Yao, D. Xiao, X. Zhu, A. F. May, W. Wu, D. H. Cobden, J.-H. Chu, X. Xu, *Nat. Mater.* **2018**, *17*, 778.
[12] a) Z. Wang, D. Sapkota, T. Taniguchi, K. Watanabe, D. Mandrus, A. F. Morpurgo, *Nano Lett.* **2018**, *18*, 4303; b) S. Albarakati, C. Tan, Z.-J. Chen, J. G. Partridge, G. Zheng, L. Farrar, E. L. H. Mayes, M. R. Field, C. Lee, Y. Wang, Y. Xiong, M. Tian, F. Xiang, A. R. Hamilton, O. A. Tretiakov, D. Culcer, Y.-J. Zhao, L. Wang, *Sci. Adv.* **2019**, *5*, eaaw0409; c) M. Alghamdi, M. Lohmann, J. Li, P. R. Jothi, Q. Shao, M. Aldosary, T. Su, B. P. T. Fokwa, J. Shi, *Nano Lett.* **2019**, *19*, 4400.
[13] a) Y. Deng, Y. Yu, Y. Song, J. Zhang, N. Z. Wang, Z. Sun, Y. Yi, Y. Z. Wu, S. Wu, J. Zhu, J. Wang, X. H. Chen, Y. Zhang, *Nature* **2018**, *563*, 94. b) Q. Li, M. Yang, C. Gong, R. V. Chopdekar, A. T. N'Diaye, J. Turner, G. Chen, A. Scholl, P. Shafer, E. Arenholz, A. K. Schmid, S. Wang, K. Liu, N. Gao, A. S. Admasu, S.-W. Cheong, C. Hwang, J. Li, F. Wang, X. Zhang, Z. Qiu, *Nano Lett.* **2018**, *18*, 5974; c) D. Weber, A. H. Trout, D. W. McComb, J. E. Goldberger, *Nano Lett.* **2019**, *19*, 5031.
[14] a) J. Stahl, E. Shlaen, D. Johrendt, *Z. Anorg. Allg. Chem.* **2018**, *644*, 1923; b) A. F. May, D. Ovchinnikov, Q. Zheng, R. Hermann, S. Calder, B. Huang, Z. Fei, Y. Liu, X. Xu, M. A. McGuire, *ACS Nano* **2019**, *134*, 4436.
[15] F. Spirovski, C. Reiner, H.-J. Deiseroth, L. Kienle, H. Mikus, *Z. Anorg. Allg. Chem. Suppl.* **2006**, *632*, 2103.
[16] a) P. E. Blöchl, *Phys. Rev. B* **1994**, *50*, 17953; b) G. Kresse, D. Joubert, *Phys. Rev. B* **1999**, *59*, 1758; c) G. Kresse, J. Furthmüller, *Phys. Rev. B* **1996**, *54*, 11169; d) J. P. Perdew, K. Burke, M. Ernzerhof, *Phys. Rev. Lett.* **1996**, *77*, 3865.
[17] G. Krier, O. Jepsen, A. Burkhardt, O. K. Andersen, The TBLMTO-ASA Program **2000**, https://www2.fkf.mpg.de/andersen/LMTODOC/LMTODOC.html.
[18] R. Dronskowski, P. E. Blöchl, *J. Phys. Chem.* **1993**, *97*, 8617.
[19] G. A. Landrum, R. Dronskowski, *Angew. Chem., Int. Ed.* **1999**, *38*, 1390.
[20] J. Stahl, L. Neudert, O. Oeckler, D. Johrendt, *Z. Anorg. Allg. Chem. Suppl.* **2016**, *642*, 994.